Fracture behavior and fracture toughness of pitch-based carbon fiber with an artificial notch introduced by a focused ion beam

Ochiai, Shojiro; Kuboshima, Shigetaka; Okuda, Hiroshi; Morishita, Kohei; Tsushima, Eiki

Fracture Behavior and Fracture Toughness of Pitch-based Carbon Fiber with an Artificial Notch Introduced by a Focused Ion Beam

Shojiro Ochiai [a], Shigetaka Kuboshima [b], Hiroshi Okuda [b], Kohei Morishita [c] and Eiki Tsushima [d]

[a] *Elements Strategy Initiative for Structural Materials, Kyoto University, Engineering Science Depts Bldg, Yoshida, Sakyo-ku, Kyoto 606-8501, Japan*

[b] *Department of Materials Science and Engineering, Graduate School of Engineering, Kyoto University, Yoshida, Sakyo-ku, Kyoto 606-8501, Japan*

[c] *Department of Socio-Environmental Energy Science, Graduate School of Energy Science, Kyoto University, Yoshida, Sakyo-ku, Kyoto 606-8501, Japan;*

[d] *FJ Composites, 701-1 Miyajima, Fuji-city, Shizuoka 416-0945, Japan*

Corresponding author:

Shojiro Ochiai, Elements Strategy Initiative for Structural Materials, Kyoto University, Engineering Science Depts Bldg, Yoshida, Sakyo-ku, Kyoto 606-8501, Japan

Tel. +81 75 753 4834

Fax: +81 75 753 4841

E-mail: shojiro.ochiai.54n@st.kyoto-u.ac.jp

Fracture Behavior and Fracture Toughness of Pitch-based Carbon Fiber with an Artificial Notch Introduced by a Focused Ion Beam

Fracture behavior and fracture toughness of pitch-based carbon fiber were studied using the fiber specimens into which an artificial mode I type straight-fronted edge notch was introduced by a focused-ion (Ga^+)-beam. Two fiber samples were used for experiment. One was the as supplied pitch-based fiber (GRANOC XN-35®, Nippon Graphite Fiber Corporation) and another was the same fiber heat-treated at 3273 K for 3.6×10^3s in argon atmosphere. The heat-treatment raised the Young's modulus from 370 to 840 GPa. The fracture toughness value of the as-supplied fiber was ~1.4 MPa·$m^{1/2}$ and the apparent fracture toughness value of the heat-treated fiber was ~4.2 MPa·$m^{1/2}$, which were estimated from the measured values of the strength (σ_f), notch depth (a) and fiber diameter (D) and correction factor. The increase in the apparent fracture toughness value due to the heat-treatment was attributed to the enhanced c-plane array and its cleavage fracture in longitudinal direction ahead of the notch tip. The analysis of the fracture strength - notch depth relation showed that the fracture of the as-supplied fiber obeys the fracture mechanical criterion and the fracture of the heat-treated fiber obeys the net stress criterion.

Keywords: pitch-based carbon fiber, heat-treatment, artificial notch, fracture behavior, fracture toughness

1. Introduction

Mechanical behavior of fiber-reinforced composites is strongly dependent on the interface. When the interface is strong, the cracks made by premature fracture of matrix and coating layer extend into fibers, resulting in low fracture strength of the composite. In order to prevent the crack extension, it is needed to cause interfacial debonding in advance of crack extension [1-4]. The condition for this has been shown around by $G_{d,c}/G_{p,c}<0.3$ where $G_{d,c}$ and $G_{p,c}$ are the critical energy release rates for interfacial debonding and fiber fracture, respectively [2-4]. The $G_{p,c}$ has one to one relation to the fracture toughness of fiber K_{Ic}. Accordingly, for design of interface to achieve high

mechanical performance of composites, the fracture toughness value of fiber is needed.

The high strength, high modulus, and low density of carbon fibers make them suitable for aerospace and sporting-goods applications [5, 6]. Among the carbon fibers, the pitch-based carbon fibers tend to have high modulus, and high thermal and electrical conductivities. For instance, the Young's modulus and thermal conductivity have reached 900 GPa and 1000 W/mK, respectively [5]. Carbon fibers consist of stacked hexagonal carbon layers, forming small coherent units (crystallites) in the stacking direction [7, 8]. The stacking direction of the layers is preferentially perpendicular to the fiber axis (axial preferred orientation) and determines the modulus of the fibers [5, 9-11]. The high degree of orientation parallel to the fiber axis, low density of defects, and high degree of crystallinity are characteristics of the fibers with high tensile modulus and high thermal and high electrical conductivity [5, 9-11].

Extensive work has been conducted to study the mechanical properties such as strength and Young's modulus of the pitch-based fibers [10-18]. However, the fracture toughness has not been revealed yet. For estimation of fracture toughness value of the small diameter fibers (5-15 μm), the difficulty arises from the small physical dimensions, due to which proper method to introduce small notches is limited. In addition, the fiber diameter is not unique, being different among the test fiber specimens. Due to the difficulties mentioned above, the fracture toughness has been estimated with indentation fracture method in combination with an empirical method, which uses the relation between the fracture toughness K_{Ic} and radius of the mirror zone in fracture surface. However, concerning the indentation fracture method, it has been shown that indentation-induced subthreshold flaws on fused silica fibers in an inert environment behave differently from the post-threshold ones, due to which consistent result cannot be obtained for the specimens with different flaw size [19, 20]. The mirror zone size

method can be applied only to the amorphous or amorphous-like fibers that exhibit mirror, mist and hackle zones in fracture surface, but not to crystalline fibers that do not show such zones. As the PAN-based fibers with relatively low Young's modulus (Torayca T300 and T800H fibers, Toray Co., whose Young's moduli were 230 and 294 GPa, respectively) show the mirror, mist and hackle zones, the fracture toughness of these fibers have been measured by the mirror zone size method to be around 1 MPa·m [14, 21]. However, as shown in Fig.1(a) and (b), the as-supplied and heat-treated pitch-based fibers employed in the present work do not show the mirror zone (details of the sample specification will be present in 2.1). The mirror zone size method cannot be applied. Accordingly, another approach is needed for estimation of fracture toughness of the pitch-based fibers.

In our preceding work [22], we introduced artificially a sharp mode I type straight-fronted edge notch in small diameter fiber with a focused-ion-beam (FIB). With this method, a sharp notch with the notch-tip radius around 25 nm could be introduced in amorphous (Tyranno-ZMI®, Ube Industries) and polycrystalline (Tyranno-SA®, Ube Industries) SiC fibers. The estimated fracture toughness of the polycrystalline SiC fiber (Tyrrano SA) with a uniform sintered structure [23] was 2.7 ±0.4 MPa $m^{1/2}$. This value was similar to the reported value [24] of 3.3 MPa·$m^{1/2}$ for the CVD-processed polycrystalline SiC fiber (SCS-6 with 140 μm in diameter, Textron, Lowell, MA). The small difference could be attributed to the difference in fabrication process, and hence microstructure. We applied this method also to two types of the alumina fibers (Al_2O_3(85 mass%)-SiO_2(15%) fiber, Altex®, Sumitomo Chemical Co., Ltd., and α-Al_2O_3 fiber, Almax®, Mitsui Mining Co., Ltd.) [25]. With this method, the fracture toughness values of the former and latter fibers were successively estimated to be 1.9 ±0.2 and 2.1±0.1 MPa·$m^{1/2}$, respectively. In both works [22, 25], the fracture toughness value

was almost independent on the notch depth in the notch depth range 0 to 2 μm. Ogiwara et al. [26] used the FIB method to introduce a sharp mode I type straight-fronted edge notch as in our former and present works and estimated the fracture toughness of the IM-600 fiber (Toho Rayon Co., Japan) to be 1.0 MPa·$m^{1/2}$.by regarding the fiber as an orthotropic material. In the present work, the FIB method above was applied to the as-supplied and heat-treated (3273 K for 3.6×10^3 s in argon atmosphere) pitch-based fibers, and the difference in fracture behavior between the fibers and its relation to fracture toughness were studied.

2. Experimental procedure

2.1 Samples

The pitch-based carbon fiber (GRANOC XN-35, Nippon Graphite Fiber Corporation, Japan) was used for test. The average diameter, tensile strength and Young's modulus of this fiber were 10.9 μm, 3.80 GPa and 370 GPa, respectively, as shown later. Hereafter, this fiber is called simply as As-S fiber. It has been known that, when the pitch-based fiber is heat-treated at ultra high temperatures (>2773K), the Young's modulus increases largely [9-11, 18, 27, 28]. In order to observe the fracture behavior and to estimate the fracture toughness of such a high modulus carbon fiber, the as supplied fiber was heat-treated at 3273 K for 3.6×10^3 s in argon atmosphere at F. J. Composite Co.[27, 28]. The heat-treated fiber is hereafter called as HT fiber for simplicity. The sizing agency was removed by acetone in a supersonic washer before the introduction of artificial notch into the fiber specimens.

2.2 Preparation of notched fiber specimens

A mode I type straight-fronted edge notch was introduced in each fiber specimen for

As-S and HT fibers with a focused-ion beam (FIB) micromachining method. Details of the procedure are shown elsewhere [22]. The outline of the procedure is presented in Fig.2. First, the fiber-ends were pasted onto a thin aluminum foil with a thickness of 11 μm. The fiber gage length for tensile testing was 10 mm. The fiber-pasted aluminum foil was placed onto a 0.3 mm thick aluminum plate. The aluminum plate was used as the beam attenuator in the later notch-forming process and also as the sample protector in the handling and as the sample carrier. The fiber-pasted aluminum foil and the aluminum plate were wrapped with specimen holders of aluminum, as shown in Fig.2(a). The assembly was then placed in the FIB (JFIB-2300, JEOL, Tokyo, Japan) apparatus. A straight-fronted edge notch (Fig.2(b)) was introduced in the fiber by the focused Ga^+-ion beam with a 55 nm spot size, at an acceleration voltage of 30 kV and probe current of 80 pA. The fiber diameter (D) and notch depth (a) of each test specimen were measured with a Scanning Ion Microscope (SIM) attached to the FIB apparatus.

2.3 Tensile test for measurement of fracture strength σ_F and Young's modulus E_f

Tensile test for the As-S and HT monofilament fibers with and without artificial notch was carried out at a crosshead speed of 8.3×10^{-6} m/s at room temperature with a universal tensile testing machine (MMT-10N-2, Shimadzu Co., Kyoto, Japan) after the measurement of diameter and notch depth for each fiber specimen. The gage length was 10 mm in the measurement of fracture strength σ_F. The test was carried out in glycerin in order to prevent the segmentation of the fiber upon fracture. Thus, the original fracture surface could be obtained for observation. The fracture surface of fibers was observed with Field Emission - Scanning Electron Microscope (FE-SEM) (X-500, Toshiba Co., Tokyo, Japan).

Another tensile test was carried out for estimation of the Young's modulus of the HT fiber. In this test, the compliance of the unnotched fiber specimens was measured under various gage lengths. The procedure to estimate the Young's modulus is outlined as follows.

The displacement measured from the moved distance of the cross-head is apparent, which is noted as ΔL_{app}. The ΔL_{app} contains the displacement of the sample itself ΔL_S and the displacement of the measurement system ΔL_M. In the present work, the following correction was made to diminish the influence of the latter deformation by estimation of the compliances of the sample and measurement system. Noting the sample length before tensile test as L_0, the displacement of the sample itself as ΔL_S and the applied load as ΔP, we can express ΔP in the form;

$$\Delta P = E_f A_f \Delta L_S / L_0 \tag{1}$$

The compliance C_M of the measurement system is expressed by $C_M = \Delta L_M / \Delta P$. As the total apparent displacement ΔL_{app} estimated from the displacement of the cross-head is given by $\Delta L_{app} = \Delta L_s + \Delta L_M$, we have

$$\Delta L_{app} / \Delta P = L_0 / (E_f A_f) + C_M \tag{2}$$

In the experiment, we took L_0=10, 20, 30, 40 and 50 mm, and carried tensile test for 10~15 fiber specimens at each L_0. Plotting the measured $\Delta L_{app}/\Delta P$ against L_0, the slope corresponds to $1/(E_f A_f)$. Substituting the measured average cross-sectional area A_f into the slope value $1/(E_f A_f)$, we have the average Young's modulus E_f of the fiber.

2.4 Estimation of fracture toughness value

The fracture strength of notched fiber (σ_{FN}), the notch depth (a) and fiber diameter (D)

were measured for each fiber test specimen. Noting the correction factor as $Y[a/D]$, which is a function of relative notch length a/D, the fracture toughness K_{Ic} is expressed by [29].

$$K_{Ic}=Y[a/D]\sigma_{FN}(\pi a)^{1/2} \quad (3)$$

where the $Y(a/D)$ is the correction factor for the present straight-fronted edge notch. In the fiber, the graphitic layer planes or basal planes are preferentially oriented parallel to the fiber axis [6, 10]. Ogihara et al.[26] have derived the $Y[a/D]$ for orthotropic material using the stiffness values of carbon fiber. In the present work, as the stiffness values of the present fiber specimens were unknown, their formula expressed by

$$Y[a/D]=9.19(a/D)^3 - 2.87(a/D)^2 +0.859(a/D) + 0.511 \quad (4)$$

was used as a first approximation. Substituting the measured values of the fiber diameter (D), notch depth (a) into Eq.(4), we had $Y[a/D]$. Then substituting the measured value of the fracture strength σ_{FN} and $Y[a/D]$ into Eq.(3), we had the fracture toughness K_{Ic}.

3 Results and Discussion

3.1 Young's modulus of the heat-treated fiber

Based on the procedure shown in subsection 2.3, the $\Delta L_{app}/\Delta P$ values were measured for 10-15 fiber specimens at the gage length L_0=10 to 50 mm. The plot of $\Delta L_{app}/\Delta P$ against L_0 is presented in Fig.3. By application of the least square method to the linear relation between $\Delta L_{app}/\Delta P$ and L_0, we had the slope $1/(E_fA_f)$=0.029 and 0.014 N^{-1} for the As-S and HT fibers, respectively. Substituting the average cross-sectional area of the fiber A_f=93 and 85 μm^2, we had E_f=370 and 840 GPa for As-S and HT fibers, respectively.

The estimated Young's modulus of the As-S fiber was close to the catalogue value of 340 GPa [30]. The Young's modulus of HT fiber, 840 GPa, was more than 2 times higher than that of the As-S one.

3.2 Appearance of the introduced notch and fracture surface of the As-S fiber

Figure 4 shows (a) SIM images of the introduced notch observed from side-surface, (b) FE-SEM images of the fracture surface of the notched As-S fiber, and (c) FE-SEM image of the fracture surface of the notched amorphous SiC fiber, for reference. As the mirror, mist and hackle zones, which appear in the amorphous fiber (Fig.4(c)), were not found in the As-S fiber (Fig.4(b)), the notch extension behavior could not be read. It is, however, noted that (i) the fiber was fractured in the cross-section in which the notch was introduced, (ii) though the fracture path could not be identified in the fracture surface of As-S fiber, the trace of the mirror-, mist- and hackle- zones in the fracture surface of amorphous SiC fiber (Fig.4(c)) shows that the fracture of fiber is caused by the introduced notch, and (iii) actually the fracture strength of the AS-S fiber was lower than the original strength and fracture obeyed the fracture mechanical criterion (when the stress intensity factor reaches the critical value, fracture occurs), as shown below.

3.3 Fracture strength and fracture toughness of the As-S fiber

In practice, the fiber diameter D was different among the fiber specimens. Thus the fracture strength σ_{FN} of the fiber specimens that are fractured by the introduced notch is dependent on a and D. In the present work, we take $Y[a/D]\sigma_{FN}$ as a unifying fracture strength parameter, which is expressed as a function only of a. Figure 5(a) shows the measured unified fracture strength $Y[a/D]\sigma_{FN}$ of the notched As-S fiber specimens plotted against notch depth a. The $Y[a/D]\sigma_{FN}$ is linearly proportional to $(\pi a)^{1/2}$ (Eq.(3))

if the fracture obeys the fracture mechanical criterion. In order to examine whether the fracture of the notched As-S fiber was caused by this criterion or not, the measured $Y[a/D]\sigma_{FN}$ values were also plotted against the corresponding $(\pi a)^{1/2}$ value, as shown in Fig.5(b). The dotted, broken and solid lines show the $Y[a/D]\sigma_{FN} - a$ curve (Fig.5(a)) and $Y[a/D]\sigma_{FN}$ - $(\pi a)^{1/2}$ linear relation (Fig.5(b)) calculated with Eqs.(3) for K_{Ic}=1.0, 1.4 and 1.8 MPa·m$^{1/2}$, respectively. The experimental results of the notched specimens are described by 1.0 ~1.8 MPa·m$^{1/2}$ range with an average of 1.4 MPa·m$^{1/2}$.

In order to examine whether the toughness values estimated from the FIB-introduced notch is affected by the notch size a and fiber diameter D or not, the estimated values were plotted against a and D, as shown in Fig.6. The present fracture toughness values are almost independent of a and D. The results in Figs.5 and 6 show that (i) the fracture of the As-S fiber obeys the fracture mechanical criterion and (ii) the FIB-introduced notch is useful for fracture toughness estimation.

For the results obtained above, the average fracture strength is described as a function of notch depth a as follows. The change of average fracture strength with a is expressed by $K_{Ic}/\{Y[a/D_{ave}]\}(\pi a)^{1/2}$ from Eq.(3), as shown with the curve AB in Fig.7. The original strength of unnotched fiber is controlled by the intrinsic defects in the fiber. The average strength $\sigma_{F0,ave}$ of unnotched (a=0 μm) fiber specimens was 3.8 GPa. The level of $\sigma_{F0,ave}$ is shown with a broken line CD. The cross-point of AB and CD is noted as E at which the notch depth a_c is 0.16 μm. In the range of $0<a<a_c$, the curve AE is higher than the $\sigma_{F0,ave}$, indicating that the fiber is fractured not by the introduced notch but by the intrinsic defects. In the range of $a_c<a$, the fiber is fractured by the introduced notch. Thus the a_c (=0.16 μm) corresponds to the notch depth at the transition from the intrinsic defects-induced fracture to the introduced notch-induced one. In the way, the fracture strength varies along CEB with increasing notch depth a.

3.4 Apparent fracture toughness and fracture behavior of HT fiber

Figure 8(a) shows the measured unified fracture strength $Y[a/D]\sigma_{FN}$ of the notched heat-treated (HT) fiber specimens, plotted against notch depth a. The experimental results of the HT fiber is apparently described with K_{Ic}=3.0 ~ 5.4 MPa·m$^{1/2}$ with an average of 4.2 MPa·m$^{1/2}$. The K_{Ic} value estimated for each fiber specimen and average for As-S and HT fibers are shown in Fig.8(b) for comparison. The fracture toughness value of HT fiber is around three times higher than that of As-S fiber. This means that the fracture toughness under tensile stress in the fiber length direction is largely enhanced by the heat-treatment that leads to higher orientation and higher graphitic order [5, 9]. However, due to the following reason, the fracture toughness of HT fiber estimated above is just apparent, while the increase in fracture resistance is surely realized by the heat-treatment.

In Fig.8, the measured $Y[a/D]\sigma_F$ values in the rectangle are not so much different to each other and they are not strongly dependent on the notch depth a, suggesting that notch extension is suppressed. Figure 9 shows FE-SEM images of the fracture surface of the notched HT fiber. The introduced notch in the HT fiber did not extend straightly ahead of the introduced notch in contrast to straight extension of the notch in As-S fiber shown in Fig.4(b). Instead, a longitudinal fracture took place, and the final fracture surface was far away from the notch-introduced cross-section.

It has been known that the modulus for basal-plane in shear has been reported to be low as 4 to 5 GPa [5, 9, 31, 32)]. In the fiber, the graphitic layer planes or basal planes are preferentially oriented parallel to the fiber axis [5, 9]. The pitch-based carbon fibers have a more regular order of the graphite planes in the sheet-like structure. Accordingly under compressive stress, the pitch based fibers with enhanced array microstructure are fractured by shearing mechanisms [5, 9, 33]. Such a mechanism

suggests that, also under applied tensile stress, mode II type fracture takes place ahead of the notch tip, in a similar manner to longitudinal cracking (splitting) ahead of the notch in the unidirectional composites [34-36]. Accordingly, the introduced notch acts to cause mode II type fracture, which suppress the model I type fracture.

In the case where the fiber is notch-sensitive and no premature longitudinal cracking occurs, the fracture mechanical criterion can be applied. Under this criterion, the strength value decreases sharply, as has been shown in the result of As-S fiber (Figs.5 and 7). On the other hand, once the longitudinal cracking takes place, the material becomes notch-insensitive. In such a case, the net stress criterion is a candidate for description of the result. This criterion has been known to describe well the fracture strength of unidirectionally reinforced composite materials with weak interface and/or weak matrix [35, 36]. According to this criterion, the fracture strength is expresses by

$$\sigma_F=\sigma_{F0}(1-A_N/A_f) \tag{5}$$

where A_N is the cross-sectional area of notched part and A_f the overall cross-sectional area of the fiber. Substituting σ_{F0}=3.7 GPa (average strength of unnotched HT fiber) and the calculated A_N/A_f as a function of a for $D=D_{ave}$ into Eq.(5), we had the σ_F - a relation for HT fiber, as shown with the broken curve in Fig.10. For comparison, the σ_F - a relation of As-S fiber (Fig.7) is shown with a sold curve. For the As-S fiber whose fracture was governed by the fracture mechanical criterion, the net stress criterion gives too high fracture strength. On the other hand, the experimental results of HT fiber in which the longitudinal cracking took place, are satisfactorily described by the net stress criterion. Based on these results, why the HT fiber kept high strength even at large notch size and why the fracture resistance (apparent fracture toughness) was so high could be accounted for from the enhanced array of basal planes which are weak in shear.

In this way, by introduction of artificial notch into small diameter fibers, the difference in fracture behavior and fracture toughness between As-S and HT fibers could be elucidated experimentally.

4. Conclusions

Fracture behavior and fracture toughness of as-supplied and heat-treated (3273 K, 3.6×10^3 s in Argon gas) pitch-based carbon fiber were studied using the fiber specimens with an artificial mode I type straight-fronted edge notch introduced by a focused-ion (Ga^+)-beam. The main results are summarized as follows.

(1) The heat-treatment raised the Young's modulus of the fiber from 370 to 840 GPa.

(2) The fracture toughness of the as-supplied fiber was estimated to be ~ 1.4 $MPa \cdot m^{1/2}$ and the apparent fracture toughness of heat-treated fiber to be ~ 4.2 $MPa \cdot m^{1/2}$. Fracture resistance is enhanced by heat-treatment.

(3) The increase in the apparent fracture toughness value due to the heat-treatment was accounted for by the enhanced c-plane array and its cleavage fracture in longitudinal direction ahead of the notch tip.

(4) The analysis of the fracture strength - notch depth relation showed that the fracture of the as-supplied fiber obeys the fracture mechanical criterion and the fracture of the heat-treated fiber specimens obeys the net stress criterion.

References

1. S. Ochiai, S. Urakawa, K. Ameyama and Y. Murakami, Experiments on fracture behavior of single fiber-brittle zone model composites, *Metall. Trans. A*. 11A, 525-530 (1980).

2. A. G. Evans, The mechanical performance of fiber-reinforced ceramic matrix composites, *Mater*. *Sci*. *Engng* A107, 227-239 (1989).

3. A. G. Evans, M. Y. He and J. W. Hutchinson, Interface debonding and fiber cracking in brittle matrix composites, *J*. *Amer*.*Ceram*. *Soc*. **72,** 2300-2303 (1989).

4. S. Ochiai and M. Hojo, Effects of pre-existent crack in souble- and gradient coatings on the crack-extension into fiber and interfacial debonding, *J. Mater. Sci.* **33**, 347-355 (1998).

5. M. L. Minus and S. Kumar, The Processing, properties, and structure of carbon fibers, J. Metals, **57,** 52-58 (2005).

6. S. Chand, Review Carbon fibers for composites, J. Mater. Sci. **35** 1303-1313 (2000).

7. A. Oberlin, Carbonization and graphitization, *Carbon*, **22,** 521-541 (1984).

8. O. Paris, D. Loidl and H. Peterlik, Texture of PAN- and pitch-based carbon fibers, *Carbon,* **40,** 551-555 (2002).

9. M. G. Northolt, L. H. Veldhuizen and H. Jansen, Tensile deformation of carbon fibers and the relationship with the modulus for shear between the basal planes, *Carbon* **29** 1267-1279 (1991).

10. Y. Huang and R.J. Young, Effect of fibre microstructure upon the modulus of PAN- and pitch-based carbon fibres, *Carbon*, **33,** 97-107 (1995).

11. Y. Huang and R.J. Young, Microstructure and mechanical properties of pitch-based carbon fibres, *J. Mater. Sci.* **29,** 4027-4036 (1994).

12. K. Naito, Y. Tanaka, J.-M. Yang and Y. Kagawa, Tensile properties of ultrahigh strength PAN-based, ultrahigh modulus pitch-based and high ductility pitch-based carbon fibers, *Carbon*, **46,** 189-195 (2008).

13. W. Johnson, The structure of PAN based carbon fibers and relationship to physical properties, in: *Strong fibers* vol.1, W. Watt and B.V. Perov (eds.), pp.389–443. Elsevier, Amsterdam (1985).

14. S. Kumar, D.P. Anderson and A.S. Crasto, carbon fibre compressive strength and its dependence on structure and morphology, *J. Mater. Sci.* **28,** 423-439 (1993).

15. R. Kulkarni and O. Ochoa: Transverse and longitudinal CTE measurements of carbon fibers and their impact on interfacial residual stresses in composites, J. Compos. Mater. **40,** 733-754 (2006).

16. F. Watanabe, S. Ishida, Y. Korai, I. Mochida, I. Kato and Y. Sakai, Pitch-based carbon fiber of high compressive strength prepared from synthetic isotropic pitch containing mesophase spheres, *Carbon,* **37**, 961-967 (1999).

17. M.C. Paiva, C.A. Bernardo and M. Nardin, Mechanical, surface and interfacial characterisation of pitch and PAN-based carbon fibres, *Carbon,* **38,** 1323-1337 (2000).

18. T. Tomioka, High tensile-strength pitch-based carbon fibers, *J. Iron Steel Inst. Japan (Tetsu to Hagane)*, **17**, 1418-1425 (1989). (In Japanese)

19. K. Jakus, J. E. Ritter, S. R. Choi, T. Lardner and B. R. Lawn, Failure of fused silica fibers with subthreshold flaws, *Non-Cryst. Solids* **102,** 82-87 (1988).

20. S. R. Choi, J. E. Ritter and K. Jakus, Failure of glass with subthreshold flaws, *J. Am. Ceram. Soc.* **73,** 268-274 (1990).

21. K. Honjo, Fracture toughness of PAN-based carbon fibers estimated from strength-mirror size relation, Carbon, **41,** 979-984 (2003).

22. K. Morishita, S. Ochiai, H. Okuda, T. Ishikawa, M. Sato and T. Inoue, Fracture toughness of a crystalline silicon carbide fiber (Tyranno SA3R), *J. Amer. Ceram. Soc.* **89,** 2571-2576 (2006).

23. T. Ishikawa, Advances in inorganic fibers, *Adv. Polym. Sci.* **178** 109-144 (2005).

24. S. Q. Guo, Y. Kagawa, Y. Tanaka and C. Masuda, Microstructure and role of outermost coating for tensile strength of SiC fiber, *Acta Mater.* **46**, 4941-4954 (1998).

25. S. Ochiai, S. Kuboshima, K. Morishita, H. Okuda and T. Inoue, Fracture toughness of Al_2O_3 fibers with an artificial notch introduced by a focused-ion-beam, *Europ. Ceram. Soc.* **30**, 1659-1667 (2010).

26. S. Ogihara, Y. Imafuku, R. Yamamoto and Y. Kogo, Direct evaluation of fracture toughness in a carbon fiber, Proceedings of 17th International Conference on Composite Materials (ICCM 17), (2009), Paper no. D6:7.

27. E. Tsushima and N. Kawamura, Manufacturing of a high thermal conductivity C/C material and development of surface coating technology, *Engineering Materials*, **46**(12), 68-72 (1998).

28. E. Tsushima and N. Kawamura: Carbon matrix metal composites, *Engineering Materials*, **47**(3), 65-68 (1999).

29. D. Broek, in: *Elementary engineering fracture mechanics,* pp. 71-77, Sijthoff and Noordhoff International Publishers, Alphen aan den Rijn, The Netherlands (1978).

30. Nippon Graphite Fiber Corp. *Catalogue* "Pitch based carbon fiber GRANOC"

31. R. Nicklow, N. Wakabayashi and H. G. Smith, Lattice dynamics of pyrolytic graphite, *Phys. Rev. B.* **5,** 4951-4962 (1972).

32. M. Grimsditch, Shear elastic modulus of graphite, J. Phys. C: *Solid State Phys.* **16** (1983)L143-L144.

33. M.G. Dobb, M.G., D.J. Johnson and C.R. Park, Compressional behaviour of carbon fibres, *J. Mater. Sci.* **25**, 829-834 (1990).

34. S. Ochiai, B. Fiedler, M. Hojo and K. Schulte, Growth of interfacial debonding in notched two-dimensional unidirectional composite under stress- and displacement-controls, *Composite Interfaces,* **7,** 459-477 (2001).

35. S. Ochiai, I. Okumura, M. Tanaka, M. Hojo, M. Sato, M. Tamura, Y. Kohtoku and T. Yamamura, Fracture behavior of notched unidirectional Si-Ti-C-O/BMAS composite, *J. Mater. Sci.* **35**, 3497-3504 (2000).

36. S. Ochiai, H. Okuda, N. Suzuki, M. Tanaka, M. Hojo and E. Tsushima: Deformation and fracture behavior of notched and unnotched unidirectional C/C-Mg composite with Young's modulus 520 GPa and strength 1GPa, *J. Mater. Sci.* **38,** 1737-1745 (2003).

Figure Captions

Figure 1. Fracture surface of (upper) as-supplied and (lower) heat-treated pitch-based carbon fibers without notch.

Figure 2. Schematic representation of the procedure to introduce an artificial straight-fronted edge notch into fiber specimen.

Figure 3. Relation of the compliance $\Delta L_{app}/\Delta P$ to gage length L_0 for the as-supplied and heat-treated carbon fibers.

Figure 4. (a) SIM images of the introduced notch observed from side-surface, (b) FE-SEM image of the fracture surface of the notched as-supplied fiber and (c) FE-SEM image of the fracture surface of the notched amorphous SiC fiber for reference.

Figure 5. Unified fracture strength $Y[a/D]\sigma_F$ of the as-supplied carbon fiber specimens plotted against (a) notch depth a and (b) $(\pi a)^{-1/2}$.

Figure 6. Estimated fracture toughness (K_{Ic}) values of the as-supplied carbon fiber plotted against (a) notch depth a and (b) diameter D.

Figure 7. Measured and analyzed change in fracture strength σ_F of as-supplied carbon fiber with increasing notch depth a.

Figure 8. (a) Unified fracture strength $Y[a/D]\sigma_F$ of the heat-treated carbon fiber specimens, plotted against notch depth a and (b) comparison of the estimated fracture toughness K_{Ic}-values of the heat-treated fiber specimens with those of as-supplied fiber specimens.

Figure 9. FE-SEM images of the fracture surface of the notched heat-treated fiber.

Figure 10. Comparison of the change in fracture strength σ_F with increasing notch depth a in heat-treated fiber with that in as-supplied fiber.

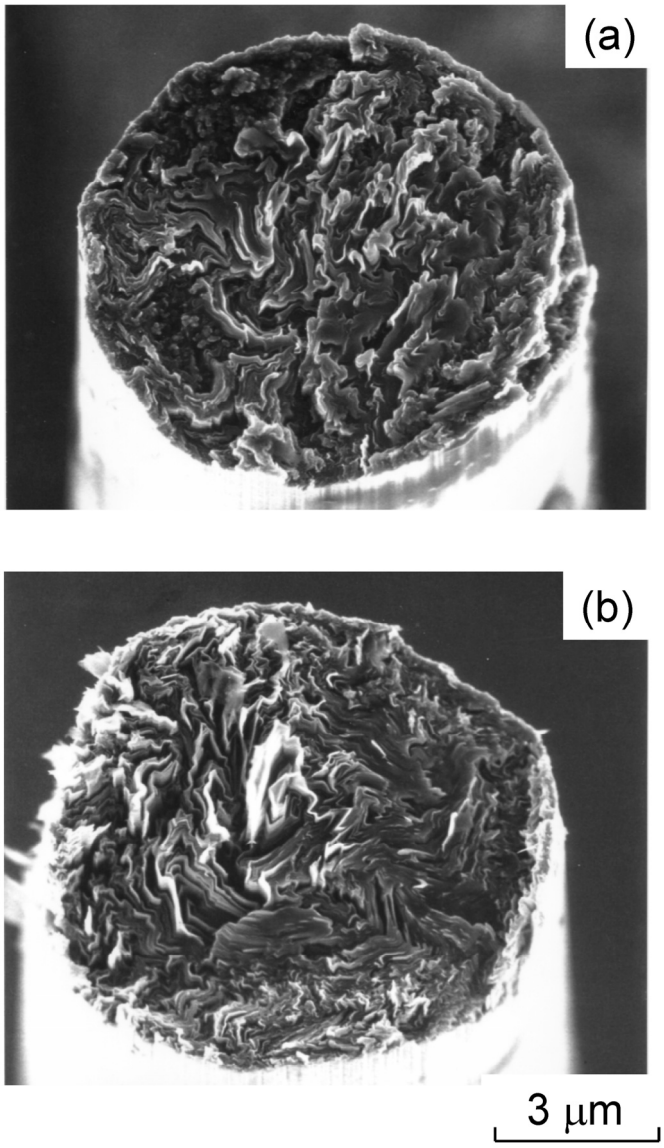

Figure 1. Fracture surface of (upper) as-supplied and (lower) heat-treated pitch-based carbon fibers without notch.

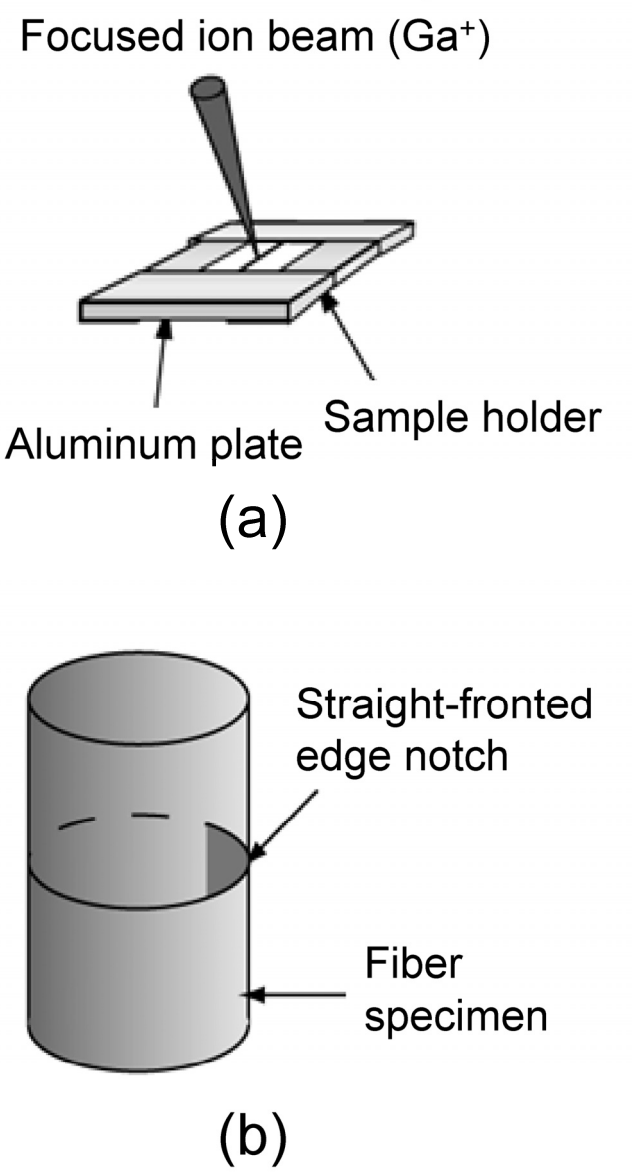

Figure 2. Schematic representation of the procedure to introduce an artificial straight-fronted edge notch into fiber specimen.

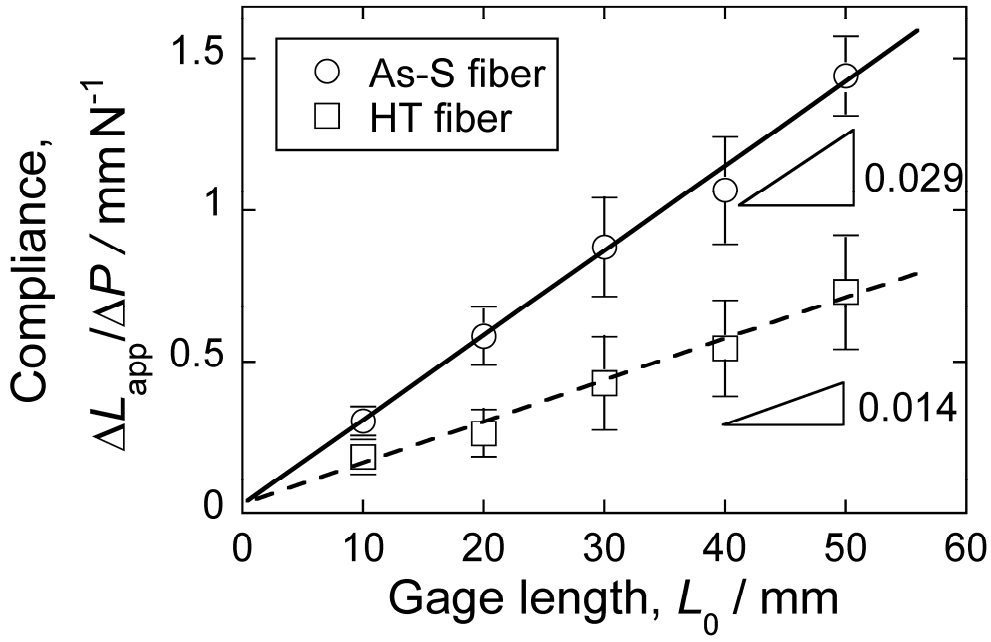

Figure 3. Relation of the compliance $\Delta L_{app}/\Delta P$ to gage length L_0 for the as-supplied and heat-treated carbon fibers.

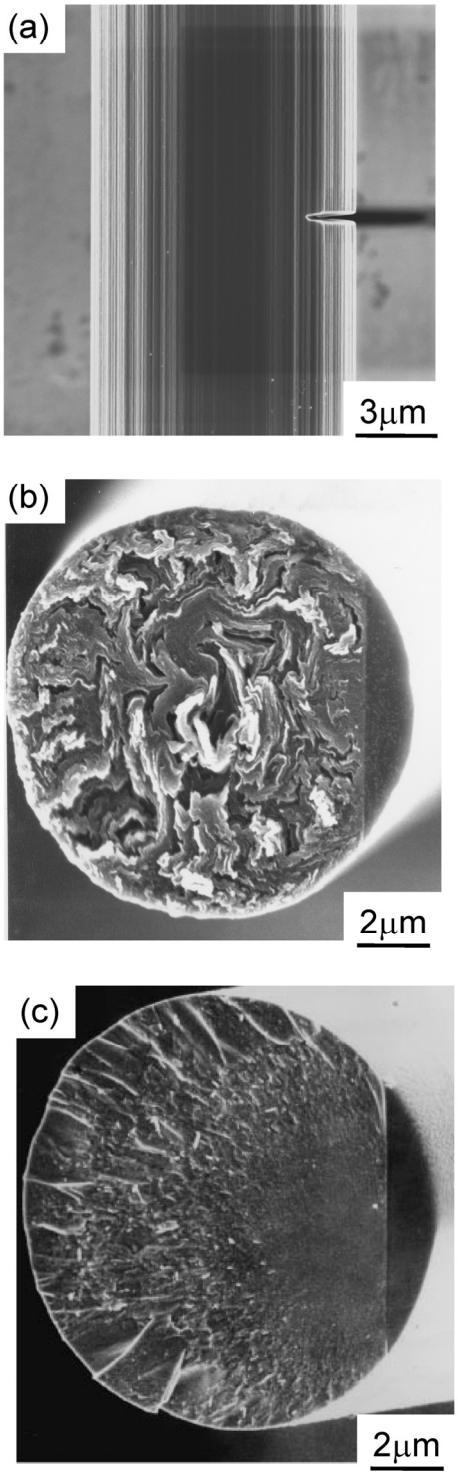

Figure 4. (a) SIM images of the introduced notch observed from side-surface, (b) FE-SEM image of the fracture surface of the notched as-supplied fiber and (c) FE-SEM image of the fracture surface of the notched amorphous SiC fiber for reference.

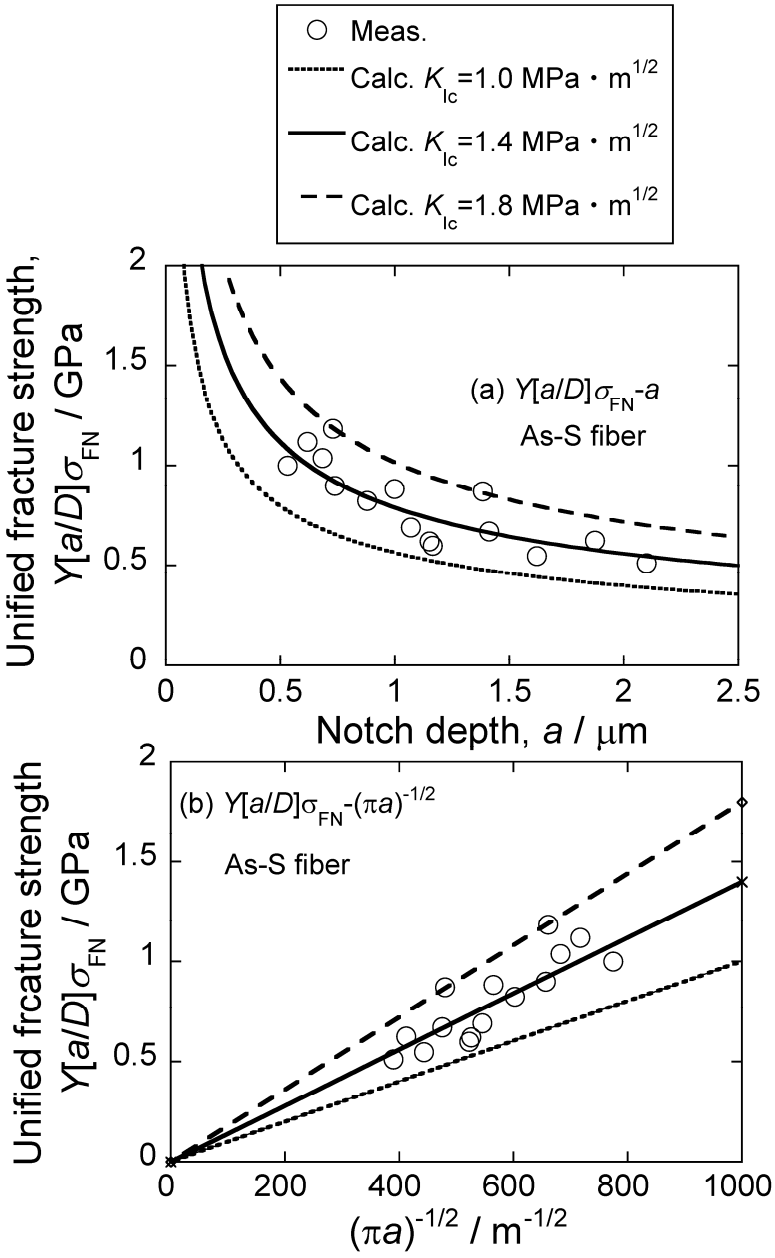

Figure 5. Unified fracture strength $Y[a/D]\sigma_F$ of the as-supplied carbon fiber specimens plotted against (a) notch depth a and (b) $(\pi a)^{-1/2}$.

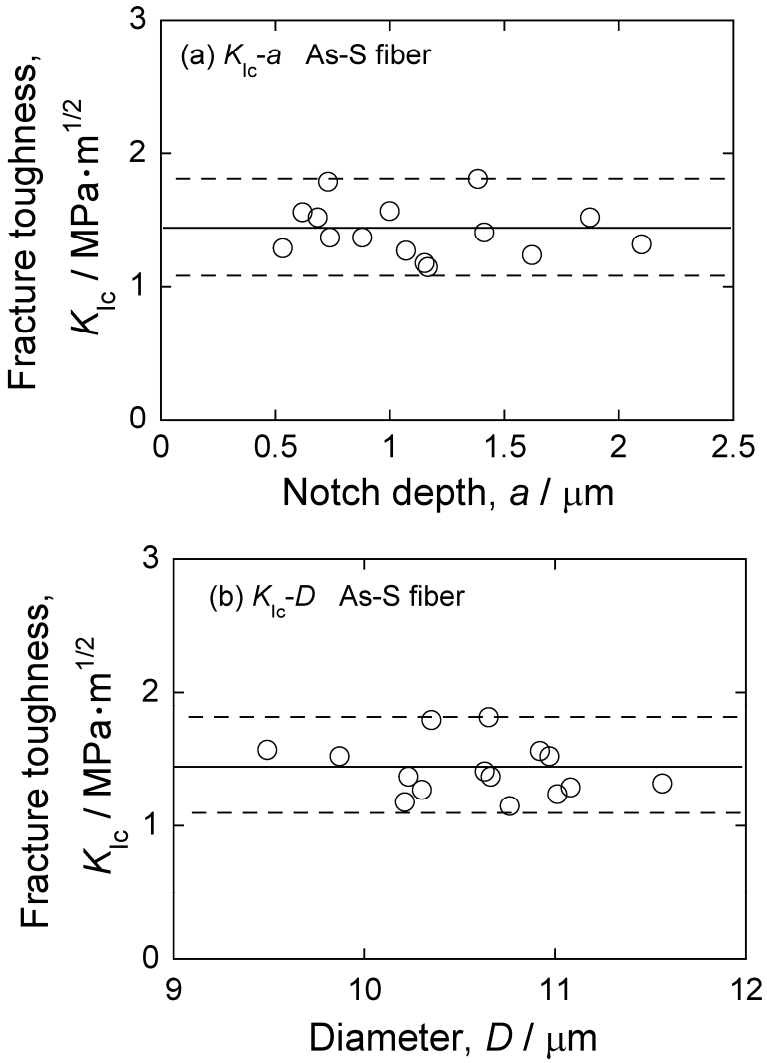

Figure 6. Estimated fracture toughness (K_{Ic}) values of the as-supplied carbon fiber plotted against (a) notch depth a and (b) diameter D.

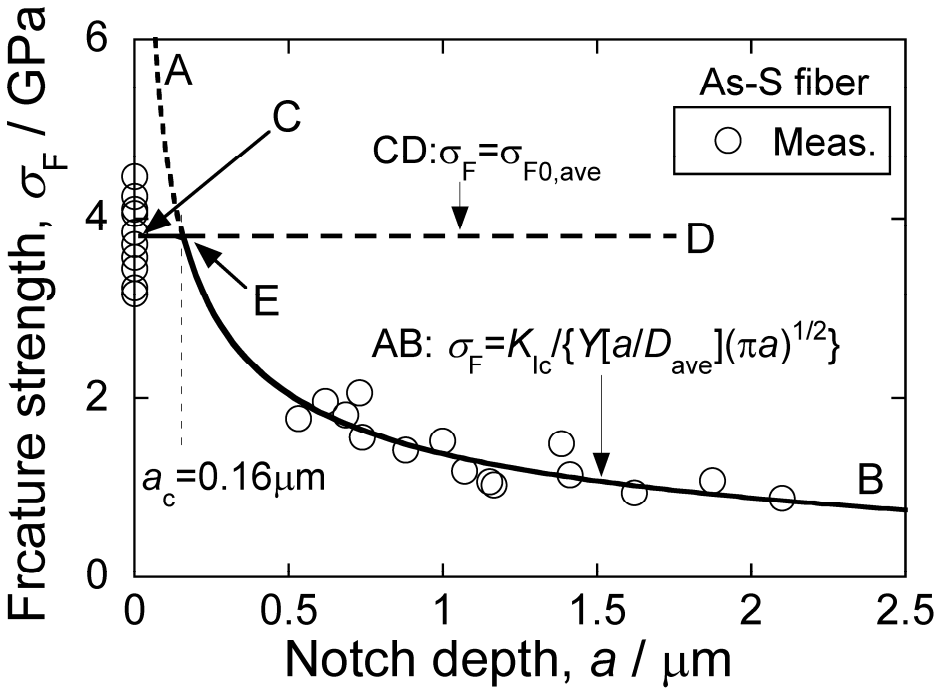

Figure 7. Measured and analyzed change in fracture strength σ_f of as-supplied carbon fiber with increasing notch depth a.

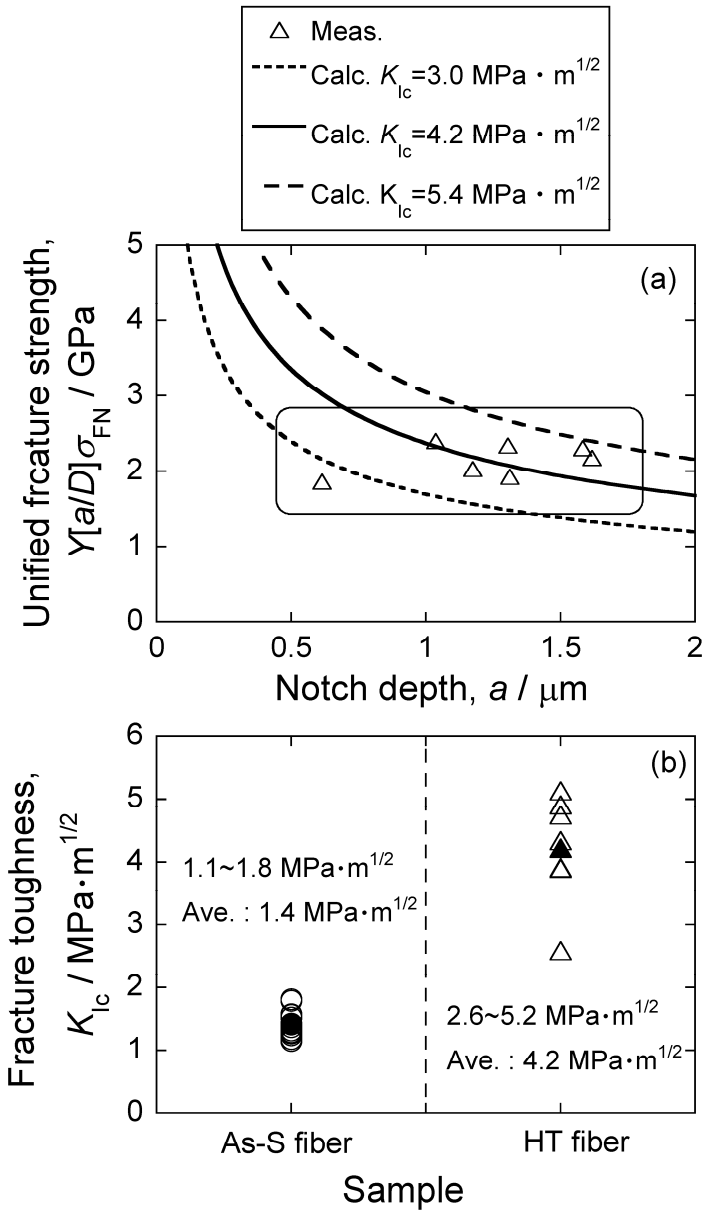

Figure 8. (a) Unified fracture strength $Y[a/D]\sigma_F$ of the heat-treated carbon fiber specimens, plotted against notch depth a and (b) comparison of the estimated fracture toughness K_{Ic}-values of the heat-treated fiber specimens with those of as-supplied fiber specimens.

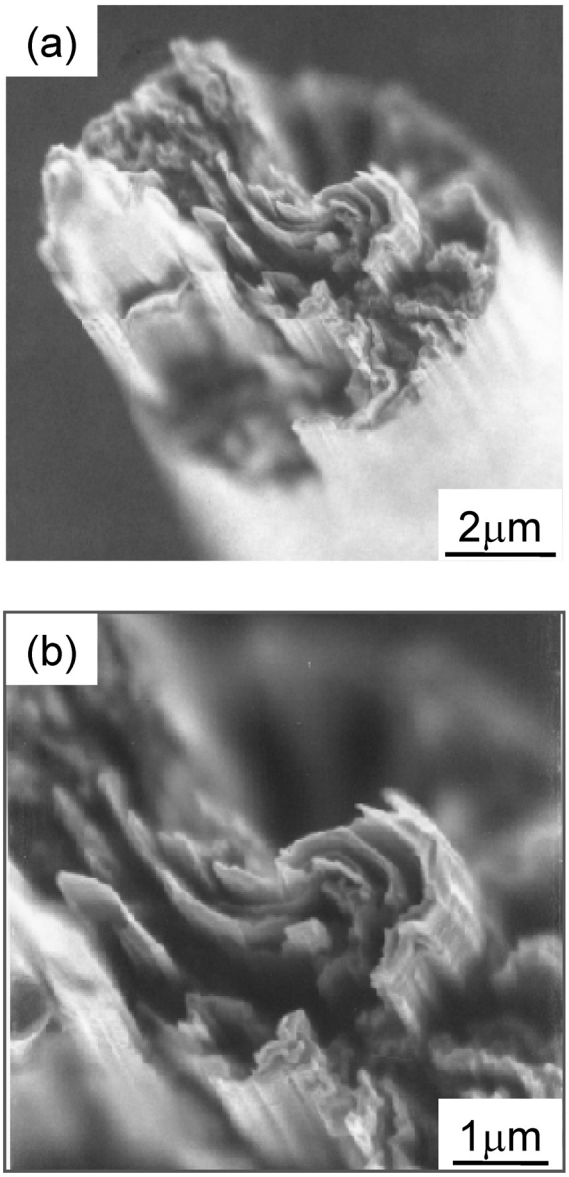

Figure 9. FE-SEM images of the fracture surface of the notched heat-treated fiber.

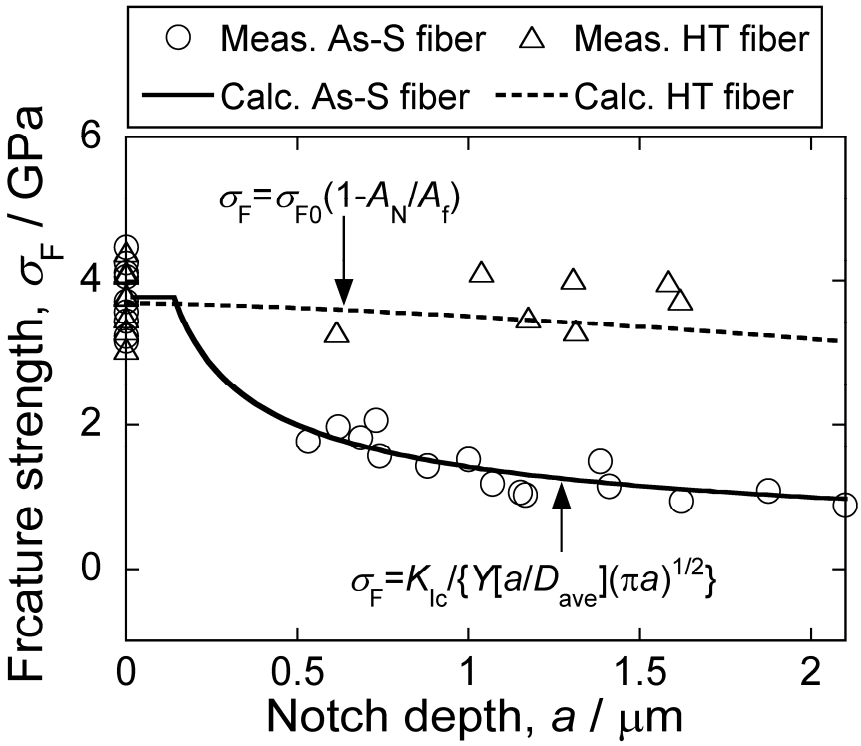

Figure 10. Comparison of the change in fracture strength σ_F with increasing notch depth a in heat-treated fiber with that in as-supplied fiber.